

Exploring uncertainty quantification for photoacoustic image reconstruction and quantitative oxygenation mapping

Original

Exploring uncertainty quantification for photoacoustic image reconstruction and quantitative oxygenation mapping / Seoni, Silvia; Scardigno, Roberto M.; Cotrufo, Bruna; Salvi, Massimo; Brunetti, Antonio; Guerriero, Andrea; Rotunno, Giulia; Buongiorno, Domenico; Vallan, Alberto; Molinari, Filippo; Meiburger, Kristen. - 13319:(2025), pp. 1-6. (Intervento presentato al convegno SPIE Photonics West - BiOS tenutosi a San Francisco (USA) nel 25-31 January 2025) [10.1117/12.3043687].

Availability:

This version is available at: 11583/2998710 since: 2025-04-01T07:19:48Z

Publisher:

SPIE

Published

DOI:10.1117/12.3043687

Terms of use:

This article is made available under terms and conditions as specified in the corresponding bibliographic description in the repository

Publisher copyright

(Article begins on next page)

Exploring uncertainty quantification for photoacoustic image reconstruction and quantitative oxygenation mapping

Silvia Seoni^{*a}, Roberto M. Scardigno^b, Bruna Cotrufo^a, Massimo Salvi^a, Antonio Brunetti^b, Andrea Guerriero^b, Giulia Rotunno^a, Domenico Buongiorno^b, Alberto Vallan^a, Filippo Molinari^a, Kristen M. Meiburger^a

^a*Department of Electronics and Telecommunications, Politecnico di Torino, Turin, Italy*

^b*Department of Electrical and Information Engineering, Polytechnic University of Bari, Bari, Italy*

ABSTRACT

Deep learning (DL) has recently been employed to enhance photoacoustic (PA) image reconstruction and quantify blood oxygenation. A significant challenge with artificial intelligence (AI) methods is the inability to quantify errors for validating predictions when the ground truth is unknown. Hence, evaluating the predictive reliability of AI models remains a significant obstacle. This study explores uncertainty quantification (UQ) in reconstructing PA images and generating oxygenation maps. 2000 images were simulated with forearm structures at three wavelengths: 750 nm, 800 nm, and 850 nm. We implemented a DNN architecture based on UNet with VGG19 as the encoder and UQ was performed using Monte Carlo Dropout during inference for 10 predictions on both simulated images and real images (in vitro and in vivo images from a volunteer). The input for the DNN architecture was the raw radio frequency (RF) data employing a 128-element linear array, while the targets were the model-based reconstructed image and the simulated oxygenation map. The study indicates that quantitative parameters can be extracted from UQ analysis on DL methods for PA image reconstruction and oxygenation mapping, providing a foundation for improved training strategies and increased robustness in employing DL methods for photoacoustic imaging applications.

Keywords: Photoacoustic imaging, Deep learning, Uncertainty Quantification, Image Reconstruction

1. INTRODUCTION

An essential component of quantitative Photoacoustic (PA) imaging involves reconstructing the initial pressure distribution (IPD) within the imaging volume using data acquired by an ultrasound array transducer [1]. Once the IPD is reconstructed and the fluence distribution estimated, the optical absorption coefficient can be derived, enabling quantitative tissue analysis. Analytical methods like back-projection, while straightforward, suffer from limitations such as reduced spatial resolution and negative pixel values in low-signal or noisy regions [2]. In contrast, model-based methods incorporate the physics of image acquisition, delivering better spatial resolution and more accurate reconstructions [2]. However, these methods are computationally intensive and often rely on iterative optimization, making them slower than analytical approaches. Another fundamental aspect of PA imaging is the ability to provide functional information using multispectral data. The main application here is the quantification of blood oxygenation, as deoxygenated and oxygenated hemoglobin present different absorption coefficients at different wavelengths.

Recently, deep learning (DL) has been employed to enhance PA image reconstruction [3], [4]. DL-based reconstruction techniques leverage large datasets to train neural networks capable of learning complex mappings from measured data to high-quality images [5]. These models offer several advantages, including learning from noisy or incomplete data and producing high-resolution reconstructions with reduced artifacts. DL methods are also faster than iterative model-based approaches, making them suitable for real-time applications [6]. DL methods have also been developed for oxygenation mapping, employing a various range of wavelengths in input [7], [8].

A significant challenge with artificial intelligence (AI) methods is the inability to quantify errors for validating predictions when the ground truth is unavailable. Hence, evaluating the predictive reliability of AI models remains a significant obstacle in several tasks, such as classification, and segmentation [9]. Several uncertainty quantification (UQ) techniques have been proposed to quantify the uncertainty of the prediction, allowing for the assessment of the robustness and reliability of the trained model. One such method is Monte Carlo Dropout, which involves applying dropout during both training and inference to generate multiple stochastic forward passes through the model [10]. This process allows for the estimation of uncertainty by producing a distribution of possible outcomes, providing insights into the model's confidence in its predictions, and helping to identify areas where the model might be less certain. This is particularly crucial for image

reconstruction and oxygenation mapping, to aim to understand and minimize such uncertainties in real applications, and for adopting novel training strategies.

In this study, we investigate the use of UQ within a deep learning-based framework that allows for the simultaneous reconstruction of PA images and oxygenation maps. Our approach uniquely combines these two tasks with uncertainty estimation, providing additional information on model reliability across different types of input data, from simulated to real images.

2. MATERIAL AND METHODS

2.1 Dataset

The Simulation and Image Processing for Photonics and Acoustics toolkit (SIMPA) [11] was used to simulate a dataset of 2000 images containing anatomical structures commonly found in the forearm. The images were generated using SIMPA leveraging a digital twin modeled after the Verasonics L11-5v probe. The parameters employed for simulating these structures followed normal or uniform distributions, with parameter ranges based on previous literature [12]. Specifically, up to three arteries (radial, ulnar, and interosseous) were simulated, along with 0, 1, or 2 accompanying veins, each with randomly assigned oxygenation values. These oxygenation values followed a uniform distribution, with arteries ranging from 0.9 to 1.0 and veins from 0.6 to 0.8. The simulations were performed using three different wavelengths: 750 nm, 800 nm, and 850 nm [13], corresponding to common imaging wavelengths employed for blood oxygenation analysis.

The dimensions of the simulated radiofrequency (RF) data are equal to 128 (number of piezoelectric elements in the simulated probe) by 789 (depth samples) for each of the wavelengths of the simulated light source, corresponding to 38x38 mm.

The dataset also comprises 2 in vivo data from a healthy subject and 8 in vitro data from SONO train vein model phantoms [14], embedded with graphite rods. The acquisitions employed a pulsed Nd:YAG laser (Phocus SE Mobile, OPOTEK, LLC, USA) as the light source, and data were acquired using the Verasonics Vantage Research Ultrasound System (USA) equipped with a 128-element L11-5v linear array probe. The laser operated at a repetition rate of 20 Hz, with a pulse width of 7 ns and the same three wavelengths were employed (i.e., 750 nm, 800 nm, 850 nm). The ultrasound system operated at a central frequency of 7.8 MHz and a sampling frequency of 31 MHz. During photoacoustic acquisitions, all 128 elements of the probe were utilized for signal reception.

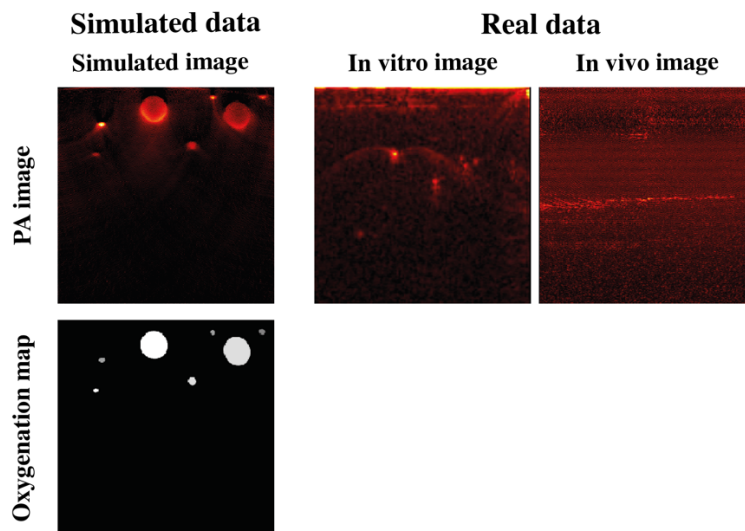


Figure 1: Example of PA image and oxygenation map of simulated data (first column) and real PA images (second column)

2.2 Deep learning model and training specifications

The deep neural network (DNN) architecture employed in this study was based on the well-known UNet model, with VGG19 serving as the encoder component. This dual-task architecture was designed to simultaneously perform two tasks: image reconstruction from RF data and generation of the corresponding oxygenation map, leveraging shared features learned during the encoding process. The network is trained over 50 epochs, with a learning rate set to 5×10^{-5} and a batch size of 8.

The input data for the DNN was the simulated RF data at the three considered wavelengths, consisting of a 3D matrix with the data acquired simulating each wavelength corresponding to one layer. The target outputs were two images: the model-based reconstructed image employing a L1 Shearlet regularization with $\lambda = 1e-5$ [15] obtained using the simulated RF data at 800 nm, and the oxygenation map that was employed during the simulation, mapping values discretized between 0 and 1 with a step size of 0.1. Both images were mapped to 256x256 pixels, which corresponds to 38x38 mm. To ensure consistency and enhance model performance, all data were normalized.

The simulated dataset was split into training, validation, and test sets with a distribution of 70%, 15%, and 15%, respectively, to ensure effective model training and evaluation while maintaining a balance between generalization and performance assessment.

The loss function used during training is a combination of two components: the first is the mean absolute error (MAE) between the optimized reconstructed image (used for the image reconstruction task) and the predicted reconstructed image, and the second is the MAE between the simulated oxygenation map (used for the oxygenation task) and the predicted oxygenation map. Unlike binary segmentation masks, the oxygenation mask contains values ranging from 0 to 1, representing varying oxygenation levels across different regions. This combined loss function ensures balanced optimization of both tasks, preventing one task from dominating the learning process while maintaining equal contribution to the model's training.

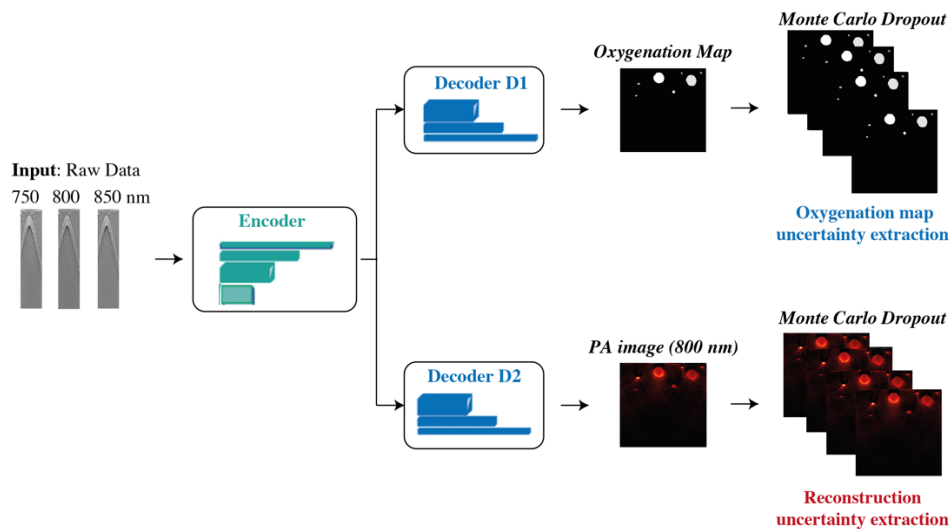


Figure 2: Illustration of a U-Net architecture with two decoders, one for PA image reconstruction (lower branch) and one for oxygenation map generation (upper branch). This network incorporates Monte Carlo Dropout (MCD) during inference in both paths to estimate uncertainty. The uncertainty in the oxygenation mask and in the PA image reconstruction is quantified as standard deviation of the MCD predictions.

2.3 Uncertainty Quantification

For UQ, Monte Carlo Dropout was applied during inference, generating 10 different predictions (N) for each input. This UQ-based approach was evaluated using three test sets: SIMPA-simulated images, in vitro and in vivo images. From the multiple reconstructions, the standard deviation of the N output was computed for each input, providing a quantitative measure of prediction uncertainty at each spatial location.

3. RESULTS

The proposed dual-task network demonstrated effective performance in both PA image reconstruction (Mean Absolute error (MAE) = 0.027 ± 0.0076) and oxygenation mapping (MAE = 0.0006 ± 0.0017) tasks in the simulated images. Figure 3 presents an example of MCD results applied to a simulated and real in vitro image from the test set. In the first row, the averages of the N simulations from the MCD are presented for both the reconstructed PA image and the oxygenation map. The first two columns display an example of a simulated image, while the last two columns show an example of an in vitro image. UQ maps provide a clearer definition of uncertainty levels, especially for simulated images. These maps offer visual information on model confidence in various image regions, with higher uncertainties often corresponding to anatomically complicated areas with low signal quality.

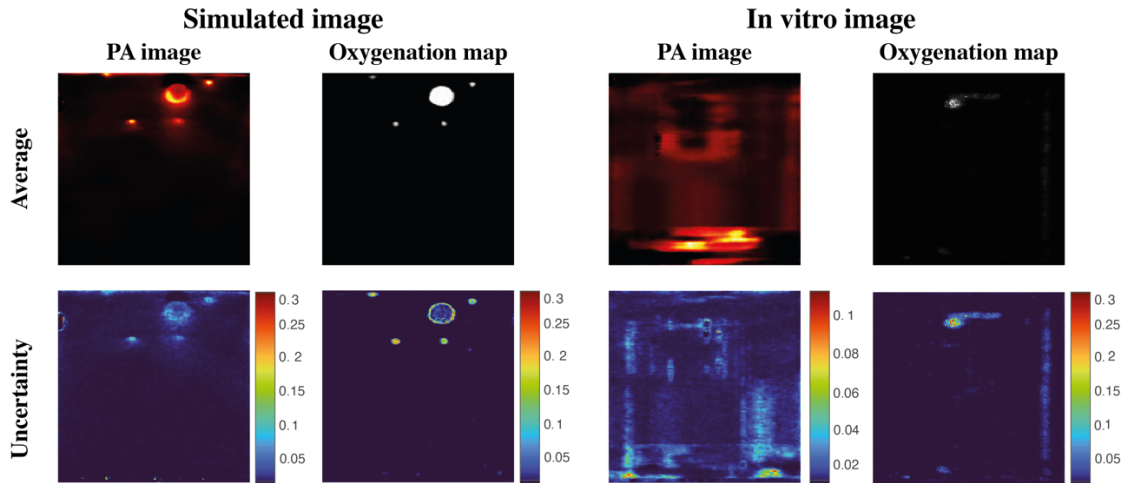


Figure 3: Example of MCD results applied to a simulated (left part) and real image (right part) from the test set. The first row shows the average of the predictions, including the overall reconstructed image (first and third column) and the oxygenation mask (second and fourth column). The second row displays the standard deviation for both tasks, with higher uncertainty observed within the targets in the reconstructed image, and increased uncertainty located at the borders of the targets in the oxygenation mask

4. DISCUSSION AND CONCLUSION

This study introduces uncertainty quantification in a dual-task framework for PA image reconstruction and oxygenation mapping, addressing a critical gap in reliability assessment of deep learning-based PA imaging. The generated uncertainty maps offer a quantitative measure of model confidence, particularly valuable in clinical scenarios where prediction reliability is essential.

The results demonstrate distinct patterns of uncertainty between simulated and real datasets. In simulated images, the oxygenation map reconstruction revealed higher uncertainty levels along the edges of the simulated veins and arteries, where structural transitions pose challenges for accurate estimation. In contrast, the uncertainty within PA image reconstructions was more uniformly distributed, including within the target region, suggesting consistent limitations in the reconstruction process across the entire image.

For real datasets, the model struggled to generalize PA image reconstruction effectively, showing expected signs of overfitting. This shortcoming was reflected in the uncertainty maps, which exhibited diffuse patterns of uncertainty across the image. Conversely, in oxygenation maps, the model demonstrated an ability to reconstruct the target while showing higher uncertainty within the target region itself.

Despite its promise, this study has some limitations. A key challenge is the limited dataset, which predominantly consists of simulated data with insufficient representation of real-world conditions. Expanding the dataset to include a greater variety of real PA images during the training phase could significantly enhance the model's generalization capabilities. Additionally, developing an uncertainty-based metric to guide model training could further refine reconstruction performance.

In future work, the estimation of uncertainty for oxygenation maps could benefit from a label-based or discrete approach. Specifically, aggregating MCD results differently could address inconsistencies in uncertainty values within individual vessels, which should ideally exhibit homogeneous uncertainty levels. This approach may provide a more reliable and interpretable measure of uncertainty, particularly for clinical applications.

The findings from this uncertainty quantification technique provide a framework for incorporating UQ measurements into PA reconstruction methods, particularly for vascular imaging applications.

ACKNOWLEDGMENT

This study was supported in part by one of the calls under the Photonics Public Private Partnership (PPP): H2020-ICT-2020-2 with Grant Agreement ID 101016964 (REAP).

This study was carried out within the “Development of inclusive quantitative photoacoustic imaging solutions enabled by ethical artificial intelligence (ImPACT-AI)” project, funded by European Union – Next Generation EU within the PRIN 2022 PNRR program (D.D.1409 del 14/09/2022 Ministero dell’Università e della Ricerca). This manuscript reflects only the authors’ views and opinions, and the Ministry cannot be considered responsible for them.

This study was carried out within the «Quantitative imaging of vascular dysregulation as a functional basis for autoimmune disorders and tumors (AI-VASCUES)» project – funded by European Union – Next Generation EU within the PRIN 2022 program (D.D. 104 - 02/02/2022 Ministero dell’Università e della Ricerca). This manuscript reflects only the authors’ views and opinions and the Ministry cannot be considered responsible for them.

This study was partially funded by the European Union – Next Generation Eu - under the National Recovery and Resilience Plan (NRRP), Mission 4 Component 2 Investment 3.3 - Decree No. 351 (09th April 2022) of Italian Ministry of University and Research - Concession Decree No. 2153 (28th December 2022) of the Italian Ministry of University and Research, Project code D93D22001390001, within the Italian National Program PhD Programme in Autonomous Systems (DAuSy)

REFERENCES

- [1] A. Rosenthal, D. Razansky, and V. Ntziachristos, “Fast semi-analytical model-based acoustic inversion for quantitative optoacoustic tomography,” *IEEE Trans Med Imaging*, vol. 29, no. 6, pp. 1275–1285, Jun. 2010, doi: 10.1109/TMI.2010.2044584.
- [2] B. Cox and M. Anastasio, “Photoacoustics Special Issue ‘Photoacoustic Image Reconstruction: Theory and Practice,’” *Photoacoustics*, vol. 30, p. 100461, Apr. 2023, doi: 10.1016/J.PACS.2023.100461.
- [3] G. Barbastathis, A. Ozcan, and G. Situ, “On the use of deep learning for computational imaging,” *Optica*, Vol. 6, Issue 8, pp. 921-943, vol. 6, no. 8, pp. 921–943, Aug. 2019, doi: 10.1364/OPTICA.6.000921.
- [4] Y. Rivenson, Y. Zhang, H. Günaydin, D. Teng, and A. Ozcan, “Phase recovery and holographic image reconstruction using deep learning in neural networks,” *Light Sci Appl*, vol. 7, no. 2, p. 17141, Feb. 2018, doi: 10.1038/lsa.2017.141.
- [5] J. Gröhl, M. Schellenberg, K. Dreher, and L. Maier-Hein, “Deep learning for biomedical photoacoustic imaging: A review,” *Photoacoustics*, vol. 22, p. 100241, Jun. 2021, doi: 10.1016/J.PACS.2021.100241.
- [6] C. Dehner, G. Zahnd, V. Ntziachristos, and D. Jüstel, “DeepMB: Deep neural network for real-time optoacoustic image reconstruction with adjustable speed of sound.”
- [7] I. Olefir, S. Tzoumas, C. Restivo, P. Mohajerani, L. Xing, and V. Ntziachristos, “Deep Learning-Based Spectral Unmixing for Optoacoustic Imaging of Tissue Oxygen Saturation,” *IEEE Trans Med Imaging*, vol. 39, no. 11, pp. 3643–3654, Nov. 2020, doi: 10.1109/TMI.2020.3001750.
- [8] P. W. Sweeney, L. Hacker, T. L. Lefebvre, E. L. Brown, J. Gröhl, and S. E. Bohndiek, “Unsupervised Segmentation of 3D Microvascular Photoacoustic Images Using Deep Generative Learning,” *Advanced Science*, vol. 11, no. 32, p. 2402195, Aug. 2024, doi: 10.1002/ADVS.202402195.
- [9] S. Seoni, V. Jahmunah, M. Salvi, P. D. Barua, F. Molinari, and U. R. Acharya, “Application of uncertainty quantification to artificial intelligence in healthcare: A review of last decade (2013–2023),” *Comput Biol Med*, p. 107441, Sep. 2023, doi: 10.1016/J.COMPBIOMED.2023.107441.

- [10] Mooney and Christopher Z., "Monte Carlo Simulation," Sage. Accessed: Aug. 23, 2023. [Online]. Available: https://books.google.it/books?hl=it&lr=&id=xQRgh4z_5acC&oi=fnd&pg=PA15&dq=monte+carlo+simulations&ots=hiPDKYwqQM&sig=6wzjxNO2bLu6cvf8muuZaE0wHIs#v=onepage&q=monte%20carlo%20simulations&f=false
- [11] "SIMPA: an open-source toolkit for simulation and image processing for photonics and acoustics." Accessed: Jan. 06, 2025. [Online]. Available: <https://www.spiedigitallibrary.org/journals/journal-of-biomedical-optics/volume-27/issue-08/083010/SIMPA--an-open-source-toolkit-for-simulation-and-image/10.1117/1.JBO.27.8.083010.full>
- [12] M. Schellenberg *et al.*, "Photoacoustic image synthesis with generative adversarial networks," *Photoacoustics*, vol. 28, p. 100402, Dec. 2022, doi: 10.1016/J.PACS.2022.100402.
- [13] A. B. E. Attia *et al.*, "A review of clinical photoacoustic imaging: Current and future trends," *Photoacoustics*, vol. 16, p. 100144, Dec. 2019, doi: 10.1016/J.PACS.2019.100144.
- [14] "Modello di vene SONOtrain - 1019637 - P120 - Ultrasound Skill Trainers - 3B Scientific." Accessed: Jan. 06, 2025. [Online]. Available: https://www.3bscientific.com/it/modello-di-vene-sonotrain-1019637-p120-3b-scientific,p_1625_27465.html
- [15] R. M. Scardigno *et al.*, "Model-Based Image Reconstruction for Linear Array Photoacoustic Imaging," *2024 IEEE Ultrasonics, Ferroelectrics, and Frequency Control Joint Symposium (UFFC-JS)*, pp. 1–4, Sep. 2024, doi: 10.1109/UFFC-JS60046.2024.10793784.